Available online at www.sciencedirect.com
ScienceDirect
Lithos 91 (2006) 331–351
LITHOS
www.elsevier.com/locate/lithos

Fluid–rock interaction in autoliths of agpaitic nepheline syenites in the Ilímaussaq intrusion, South Greenland☆

Johannes Schönenberger, Michael Marks, Thomas Wagner, Gregor Markl *

Institut für Geowissenschaften, AB Mineralogie und Geodynamik, Eberhard-Karls-Universität, Wilhelmstrasse 56, D-72074 Tübingen, Germany

Received 31 May 2005; accepted 13 March 2006
Available online 26 May 2006

Abstract

Within the 1.16 Ga old Ilímaussaq intrusion, up to 700 m large autoliths occur in one stratigraphic unit of the layered floor series of agpaitic nepheline syenites (kakortokites). These autoliths consist of two different rock types: augite syenite and naujaite (agpaitic nepheline syenite). All three rock types show a number of alteration features related to the entrapment of the autoliths in the kakortokite magma caused by the interaction with a fluid phase.

In the kakortokites, the oxidation of primary arfvedsonite to aegirine and fluorite is restricted to the close proximity to the autoliths. Close to the surrounding kakortokite, the primary mafic phases of the augite syenites (augite, fayalite, Fe–Ti oxides) are completely replaced by arfvedsonite, aenigmatite, biotite, aegirine and fluorite. The decomposition of primary hastingsite to spectacular aegirine–augite–nepheline–aenigmatite symplectites can be observed up to several meters inside the autoliths. Additionally, fluorite formed at grain boundaries of primary nepheline. In the naujaite autoliths, primary arfvedsonite is replaced by aegirine–biotite intergrowths and abundant aenigmatite is occasionally replaced by Ti-rich aegirine and Fe–Ti oxides.

The mineral reactions in the autoliths are used to decipher details of the late to post-magmatic processes in a peralkaline syenitic intrusion. Mineral equilibria record an evolution governed by falling temperature (620 to ca. 500 °C) and increasing relative oxygen fugacity from FMQ+1 to above FMQ+4. Quantification of the observed mineral reactions reveals the infiltration of the autoliths with an oxidizing fluid phase rich in Na and F and minor addition of K. Volatiles (H and F) and in some cases also Fe, Ti and Ca (±Mg) released from primary autolith phases were mainly just relocated within the autoliths.

Keywords: Ilímaussaq; Isocon-method; Fluid–rock interaction; Element-mobility; Peralkaline; Autoliths

1. Introduction

The chemical evolution of (per-)alkaline liquids has attracted considerable interest in the last decades, as such liquids are capable of concentrating rare elements like Zr, Nb, Ta, REE or Th to very high concentrations (e.g. Kogarko, 1980; Drysdall et al., 1984; Bowden, 1985; Sørensen, 1992, 1997). Specifically, the unmixing of a fluid phase from a crystallizing melt and its autometasomatic behaviour are important for the redistribution of elements within a solidifying magma chamber. These effects can cause replacement of primary magmatic by secondary mineral assemblages. Peralkaline igneous complexes are well known for late-magmatic processes involving aqueous fluid phases ("fenitization"; e.g. Rock, 1976; Kunzendorf et al., 1982; Morogan, 1989; Salvi and Williams-Jones, 1990). However, the details of fluid composition, fluid–melt–

☆ Contribution to the mineralogy of Ilímaussaq No. 128.

* Corresponding author. Tel.: +49 7071 2972930.
E-mail address: markl@uni-tuebingen.de (G. Markl).

0024-4937/$ - see front matter © 2006 Elsevier B.V. All rights reserved.
doi:10.1016/j.lithos.2006.03.024

mineral relations and the reaction mechanisms may be different in each case. Understanding the mobility of elements during late-magmatic interaction is important for the quantification of such processes. Depending on specific conditions of the fluid such as pH and fugacities (O, F), certain elements are mobilized while other elements are added during alteration. For example, HFSE and REE are generally immobile in hydrothermal alteration processes, but they may be highly mobile in peralkaline systems (Salvi et al., 2000). Fluid assisted remobilization processes may be of great importance for the geochemical evaluation of e.g. magma source, contamination or assimilation processes and they may also lead to economically important enrichment of elements such as Nb, Ta or REE.

The present study deals with reaction textures developed in autoliths of the peralkaline Ilímaussaq complex, South Greenland. Here, the interaction between evolved melts and late-stage fluids with earlier crystallized rocks of the same magmatic event can be studied in detail and the development of secondary mineral assemblages allows us to quantify fluid–rock interaction and to investigate the late-stage (re-) mobilization of elements such as F, Fe, Na etc. We discuss the interaction between autoliths, a fluid phase and the surrounding magma in the context of mineralogy and intrinsic parameters of the intrusion.

2. Geological setting and previous work

The Ilímaussaq intrusion belongs to the 1.35–1.14 Ga Gardar province (Upton et al., 2003). The formation of the 1.16 Ga old intrusion (Fig. 1a–c) is described as a succession of three magma batches from one single mantle source (Larsen and Sørensen, 1987; Marks et al., 2004), which intruded successively to 3–4 km depth (Konnerup-Madsen and Rose-Hansen, 1984). The first batch crystallized an augite syenite which was followed by a peralkaline granite. The nepheline syenites of the third and main magma pulse can be divided into roof cumulates (pulaskite, foyaite and naujaite), floor cumulates (kakortokites) and volatile-rich and highly mobile rocks of a sandwich horizon (lujavrites) which represent the residual liquids (Larsen and Sørensen, 1987). All agpaitic nepheline syenites are composed of arfvedsonite, aegirine, alkali feldspar, nepheline, eudialyte, sodalite and fluorite in different modal compositions. The Ilímaussaq intrusion was the subject of many studies in the last decades and their mineralogy, petrology and geochemistry are well known (e.g. Ferguson, 1964; Engell, 1973; Larsen, 1976, 1977, 1981; Larsen and Sørensen, 1987; Bailey et al., 2001; Markl et al., 2001; Sørensen, 2001; Marks et al., 2004). The evolution of intrinsic parameters within the Ilímaussaq complex was established in detail by Markl et al. (2001) and Marks and Markl (2001): crystallization temperatures range from >1000 °C in the augite syenites to <500 °C in the lujavrites. Relative oxygen fugacity decreased during crystallization of the augite syenite from ΔFMQ=−1 to ΔFMQ=−4 and increased during the crystallization of the agpaitic nepheline syenites to values of about ΔFMQ +2 to +4.

The kakortokites crop out as a 280 m thick rock series. The lower part is spectacularly layered (Fig. 2a) and can be divided into 29 units, numbered from −11 to +17 (Bohse et al., 1971). Each unit is characterized (from bottom to top) by a black arfvedsonite-rich, a red eudialyte-rich and a white alkali feldspar-rich layer (Bohse et al., 1971). During the crystallization of the layered kakortokites, the roof of the magma chamber collapsed and earlier crystallized fragments (autoliths) of augite syenite and naujaite sank into the kakortokitic magma (e.g. Larsen and Sørensen, 1987). The resulting autoliths are concentrated in the 20 m thick white layer of unit +3 (Ferguson, 1970; Bohse et al., 1971). The autoliths are up to 700 m in diameter and their contacts are well exposed.

3. Sample descriptions and petrography

Three sample series out of eight sampled (Figs. 1c and 2a) with a total of 17 samples (series IV, VI and VIII) covering a profile from the interior of the autoliths into the surrounding kakortokites were investigated in detail to quantify magma–fluid–autolith interactions. They are described in Table 1. Up to 2 m thick pegmatites are developed around some autoliths (Fig. 2b; Ferguson, 1970), while they are not present around others. The formation of these pegmatites is the only direct indication for melt–autolith interaction. There is neither evidence of partial melting, nor any melt inclusions or small veins penetrating the autoliths.

3.1. Original rock types not affected by fluid-autolith interaction

Kakortokites consist of modally variable amounts of primary alkali feldspar laths, arfvedsonite, aegirine, eudialyte, nepheline and fluorite (Fig. 3a). Arfvedsonite is commonly euhedral (up to 4 mm diameter) whereas the less frequent aegirine occurs interstitially. Interstitial nepheline is commonly altered to analcime, sodalite or natrolite. Other decomposition products of primary

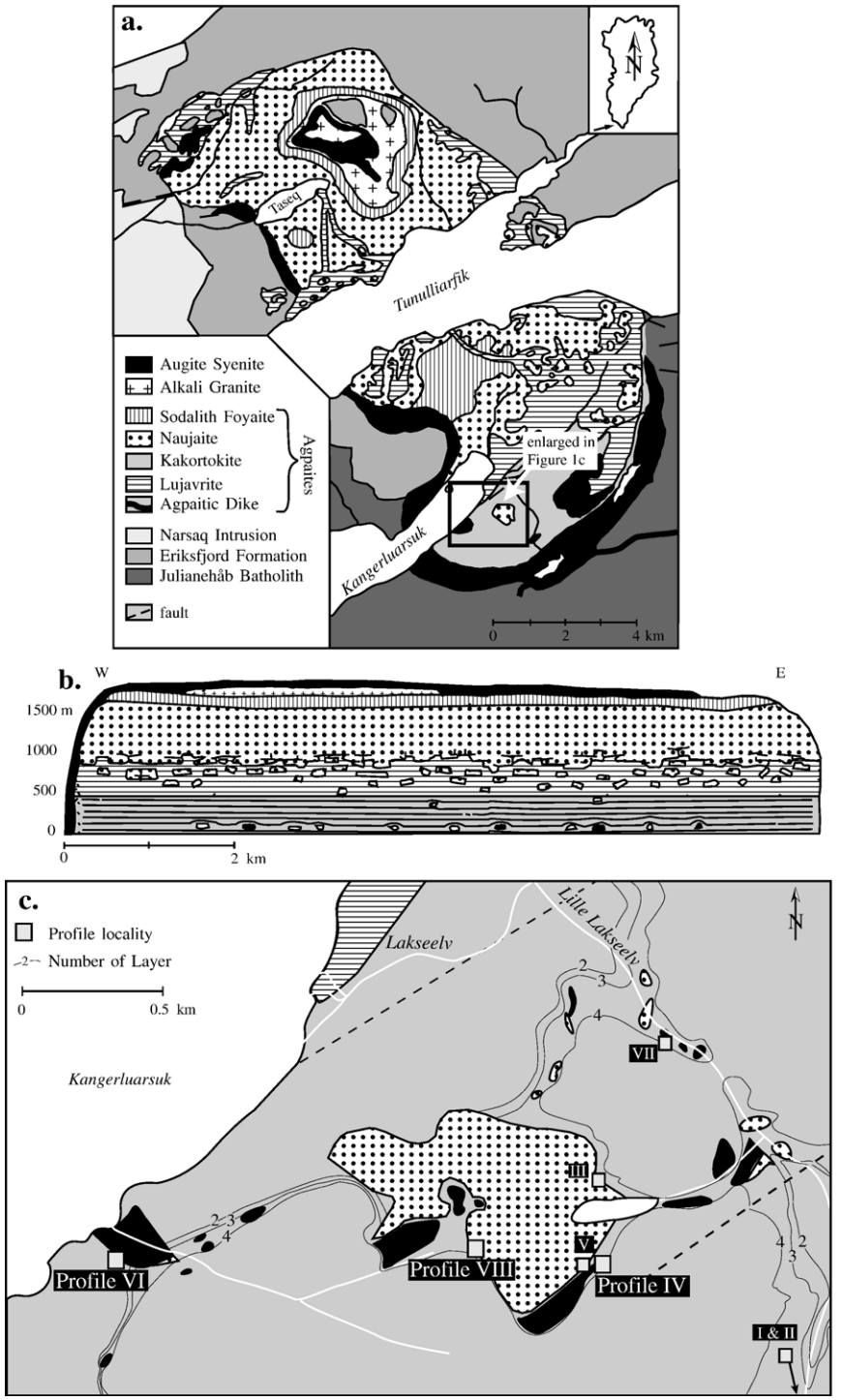

Fig. 1. (a) Geological map of the Ilímaussaq intrusion after Ferguson (1964). (b) Schematic cross section of the intrusion from W to E after Andersen et al. (1981). (c) Enlargement of the southern part of the Ilímaussaq complex (Bohse et al., 1971). The eight sample profiles taken from different autoliths are indicated.

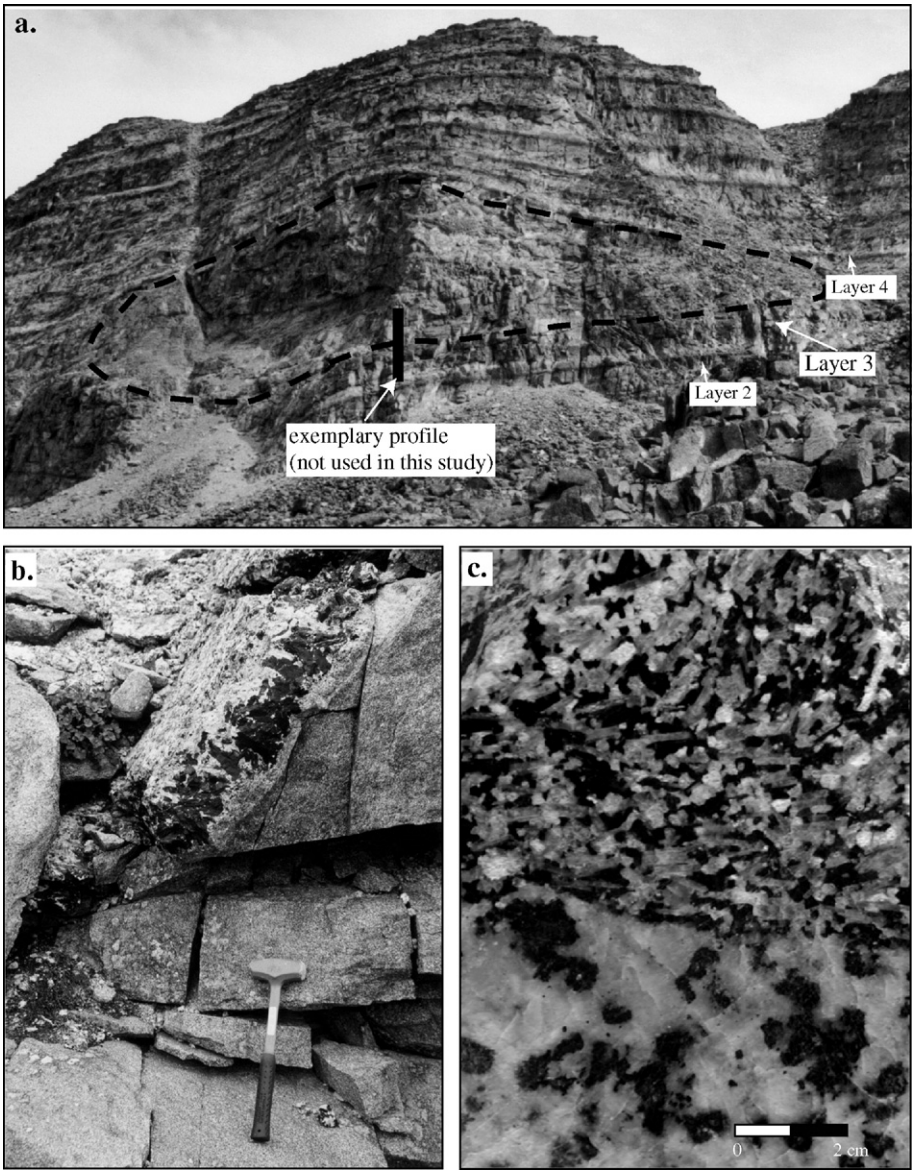

Fig. 2. (a) Photograph of a part of the spectacularly layered kakortokite series of the Ilímaussaq intrusion. The layers are bent above an augite syenite autolith that is marked with the dotted line. The height of the cliff is approx. 100 m. (b) Contact relation between kakortokite (lower right part) and augite syenite autolith (upper left). The two rocks are separated by a 25 cm thick pegmatite with large arfvedsonite and feldspar crystals (profile IV). (c) Polished specimen (profile VI) which exhibits a razor-sharp contact. In the upper kakortokitic part, aligned feldspar laths (white color) and arfvedsonites (black) are parallel to the contact. The augite syenite (lower part) is characterized by aggregates of mafic minerals (black areas) in a feldspar matrix.

minerals are fluorite, pectolite, biotite and catapleiite (Ferguson, 1964).

Augite syenites consist of alkali feldspars and minor interstitial nepheline (Fig. 3b). The mafic phases (clinopyroxene, olivine and Fe–Ti oxides) and apatite are concentrated in aggregates. Subordinate amphibole and biotite occur as rims around the other mafic mineral phases and are late hydrothermal reaction products (Larsen, 1981; Marks and Markl, 2001).

Naujaites show a poikilitic texture dominated by euhedral sodalite grains and interstitial amphibole, aegirine, eudialyte or feldspar (Fig. 3c). Fluorite, nepheline, analcime, natrolite and catapleiite are rare.

Table 1
Sample profiles used in the present study

Sample	Rock type	Distance to contact	Descriptive remarks
Profile IV			
XL27	Kakortokite	1 m	Augite syenite autolith; 400 * 50 m. Marginal 1 m thick pegmatite (arfvedsonite/alkali feldspar).
XL29	Kakortokite	Contact area	
XL31	Augite syenite	0.1 m	
XL32	Augite syenite	1 m	
XL33	Augite syenite	2.5 m	
XL34	Augite syenite	3.5 m	
Profile VI			
XL57	Kakortokite	1.5 m	Augite syenite autolith; ~400 m diameter. Razor-sharp contact (Fig. 2c). No field evidence of an alteration of kakortokite or augite syenite. Alignment of feldspar laths in the kakortokite parallel to the contact.
XL54	Kakortokite	Contact area	
XL55	Kakortokite/ augite syenite	Contact area	
XL53	Augite syenite	0.1 m	
XL51	Augite syenite	2.5 m	
XL50	Augite syenite	4 m	
Profile VIII			
XL75	Kakortokite	3 m	Naujaite autolith; ~700 m diameter. Transition zone from naujaite to kakortokite. Kakortokite exhibits a poikilitic texture which is characteristic of naujaites.
XL77	Kakortokite	1 m	
XL78	Kakortokite	0.2 m	
XL82	Naujaite	2 m	
XL83	Naujaite	4 m	

3.2. Kakortokite–augite syenite interaction

Fig. 6a schematically summarizes the alterations observed in the kakortokites and augite syenites. Generally, the *kakortokites* of both augite syenite–kakortokite profiles show little macroscopic evidence of fluid–autolith interaction. However, kakortokite sample XL29 (profile IV) shows complete replacement of primary arfvedsonite by aegirine and fluorite. Additionally, aegirine grains are penetrated by small albite veins. Eudialyte is missing. In the kakortokitic part of sample XL55 (profile VI; sharp contact), the slight enrichment of fluorite and aenigmatite grains may be related to the proximity of the autolith.

The *augite syenites* exhibit different reaction textures which are observed: (1) up to a few centimeters, (2) up to several meters inside the autoliths. Both types are now described in detail.

At the contact (sample XL55, Fig. 2c) the primary augite syenite texture is completely modified:

- In contrast to all other augite syenites, amphibole is the dominant mafic mineral phase, whereas clinopyroxene is subordinate. The amphiboles are variable in grain size: large grains (<1 mm) with many fluorite inclusions (Fig. 4a), grains without any inclusions and small (<50 μm), partially euhedral grains. The latter form either aggregates in the feldspar matrix or they are grouped around relics of Fe–Ti oxides, olivines, aenigmatites and biotites (Fig. 4b). The small amphibole grains are commonly rimmed by secondary aegirine and intergrown with nepheline.

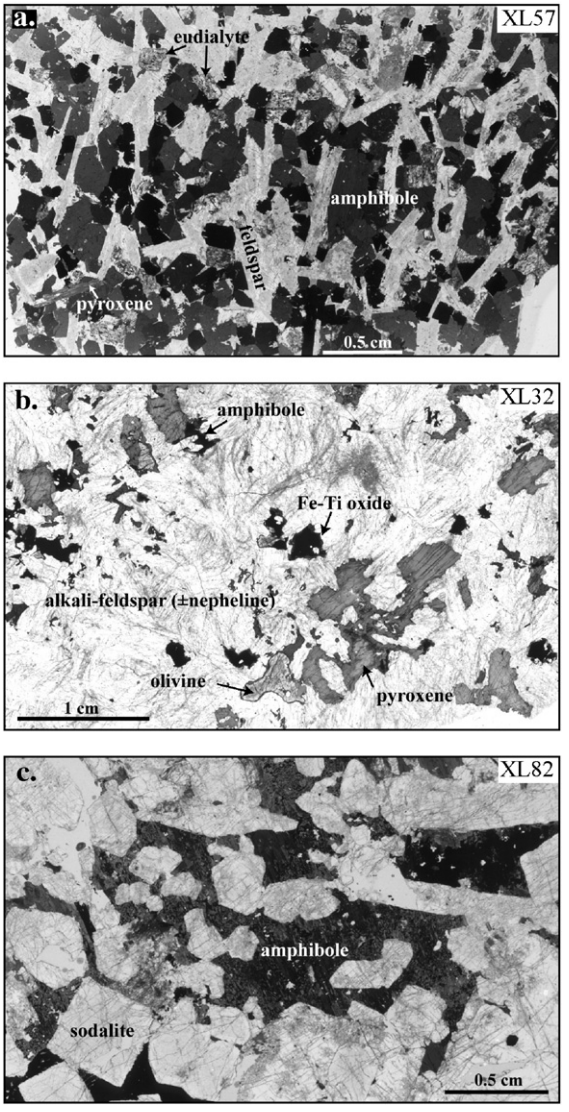

Fig. 3. Three thin section images of the rock types examined in this study. (a) Texture of a typical kakortokite. The rock is dominated by alkali feldspar laths, arfvedsonite and eudialyte. (b) The augite syenite is characterized by a matrix of alkali feldspar with minor amounts of interstitial nepheline. Mafic minerals comprise pyroxene, Fe–Ti oxides, olivines and amphibole. (c) Euhedral sodalite dominates the poikilitic texture of the naujaite. Arfvedsonite and feldspar occur interstitially.

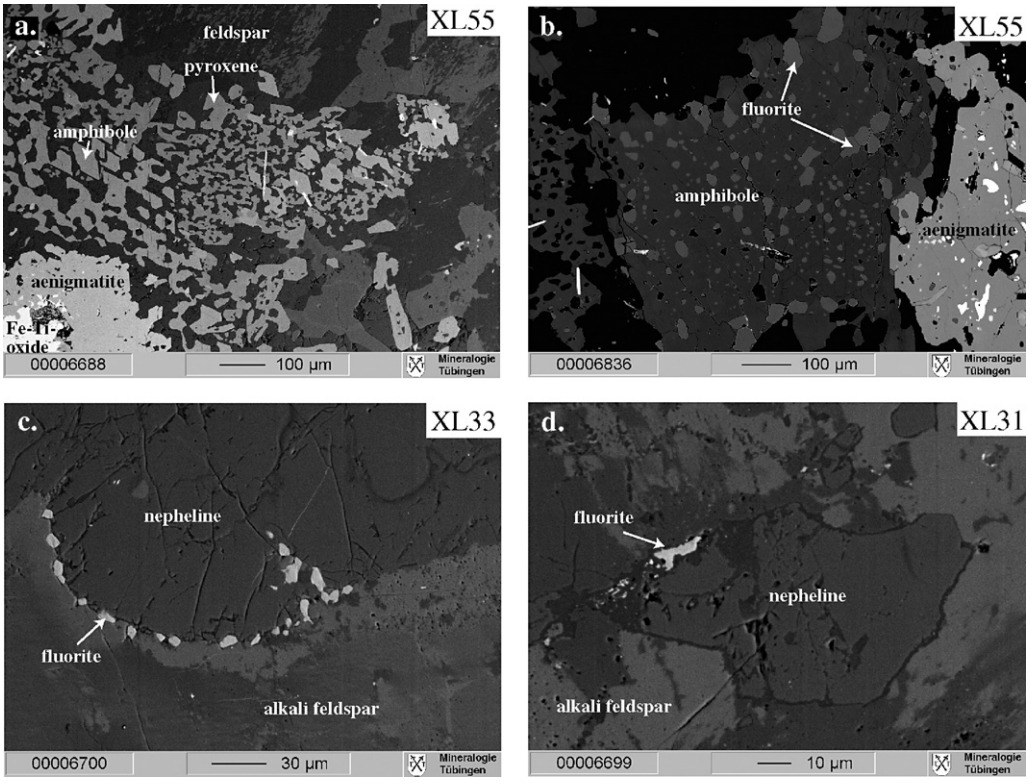

Fig. 4. (a) and (b) are BSE images from the augite syenitic part of sample XL55 which represents the sharp contact between augite syenite and kakortokite (Fig. 2c). (a) shows the sequence Fe–Ti oxide (lower left corner)–aenigmatite–amphibole–pyroxene (upper right). (b) displays another type of amphibole grains with many small fluorite inclusions. (c) and (d) show interstitial primary nepheline grains with fluorite along their grain boundaries.

- Olivine is only present as iddingsitized relics and Fe–Ti oxides are largely replaced by aenigmatite (Fig. 4b).
- Fluorite is concentrated along grain boundaries of nepheline and alkali feldspars. It is more abundant than in the other augite syenite samples.

Further from the contact, other reaction textures are observed in both augite syenite profiles (XL31–34; XL53):

- Primary amphibole has decomposed to pyroxene–nepheline±aenigmatite symplectites (Fig. 5a–d). The reaction textures may involve additional biotite or Fe–Ti oxides as reacting phases (Fig. 5c).
- Small fluorite grains (<10 µm) are developed along grain boundaries between primary nepheline and alkali feldspar (Fig. 4c and d) and rarely along cracks through these minerals.
- The replacement of primary nepheline and alkali feldspar by analcime is a common feature in the autoliths, which however, also occurs in non-autolithic augite syenite (Marks and Markl, 2001).

In profile VI, the intensity of amphibole decomposition decreases with distance from the contact whereas no correlation is obvious in profile IV.

3.3. Kakortokite–naujaite interaction

Kakortokite samples XL77 and XL78 (profile VIII) display similar alteration features as kakortokites from profile IV. Primary arfvedsonite is replaced by poikilitic aegirine and fluorite.

In the *naujaites*, primary amphibole is replaced by symplectitic intergrowths of aegirine and biotite (Fig. 5e). In sample XL82, all amphibole is completely replaced by aegirine or aenigmatite. Aenigmatite is very dominant and partly replaced by an assemblage of pyroxene, Fe–Ti oxides (Fig. 5f) and/or biotite. Secondary fluorite grains are associated with all these reaction textures. Sodalite, feldspar and nepheline are occasionally replaced by analcime and/or natrolite. The

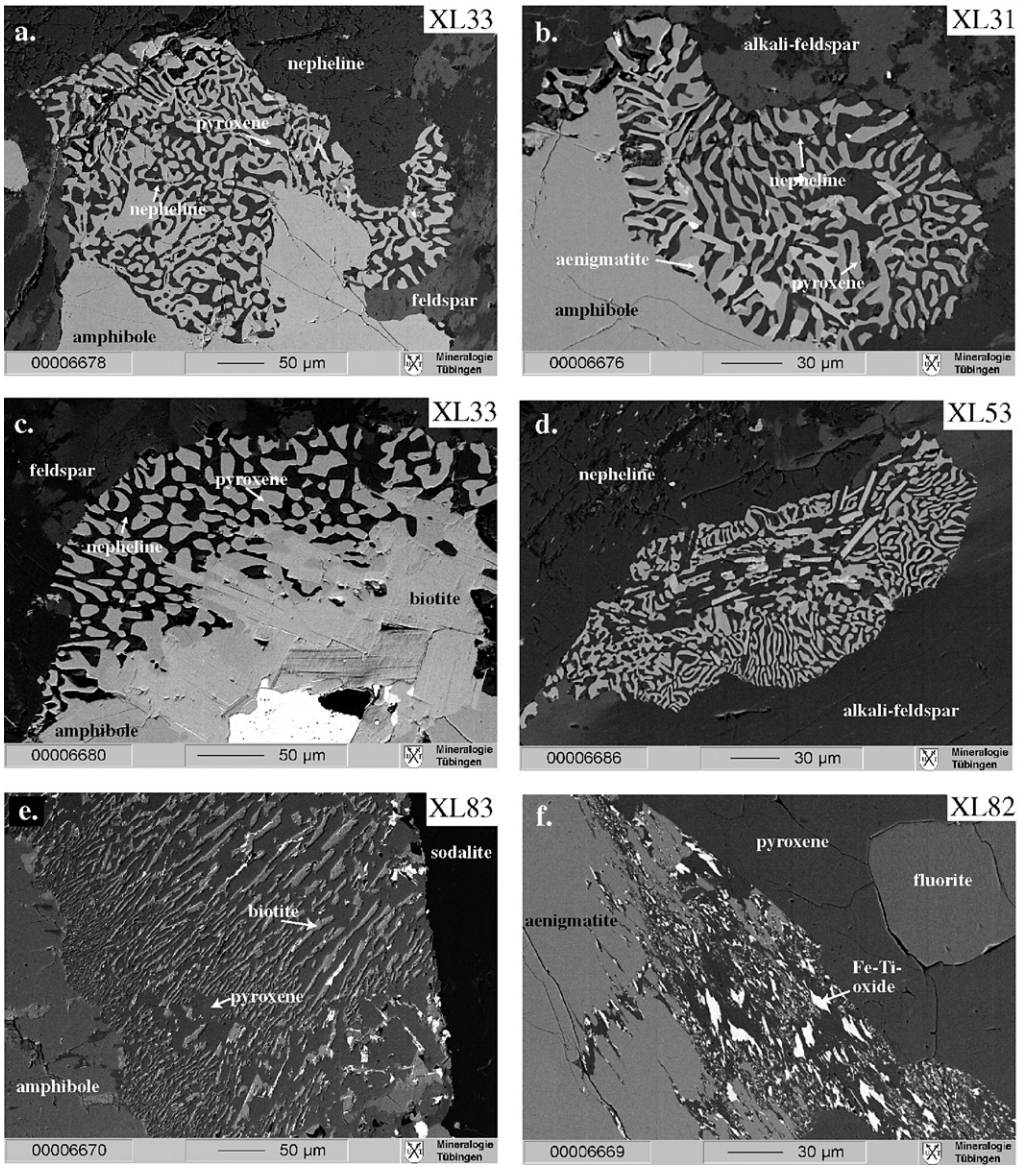

Fig. 5. Different reaction textures in augite syenite (a–d) and naujaite (e–f). (a–d) show BSE images of reaction textures of the amphibole decomposition in the augite syenite according to reaction (7). (a) Two-phase-symplectite consisting of pyroxene and nepheline. (b) Three-phase-symplectite with additional aenigmatite in the product phases. (c) A more complex reaction texture where mica and/or Fe–Ti oxides were possibly involved in the reaction. (d) Texture, where the reaction has gone to completion. (e) Amphibole decomposition to pyroxene–mica intergrowths in naujaite sample XL83. (f) is a picture of the common decomposition of aenigmatite to aegirine and Fe–Ti oxides.

alterations observed in and around the naujaite autolith are schematically shown in Fig. 6b.

4. Mineral chemistry

4.1. Analytical techniques

Minerals were analyzed using the Jeol 8900 electron microprobe of the Institut für Geowissenschaften, Universität Tübingen, using natural and synthetic standards. Beam current was 15 nA and acceleration voltage 15 kV. Peak counting time ranged between 16 and 60 s for major and minor elements, respectively. Background counting times were half the peak time. We used a focused electron beam for all minerals except feldspar, nepheline and analcime which were analyzed with a beam diameter between 2 and 20 µm depending on grain size and exsolution textures to avoid alkali loss.

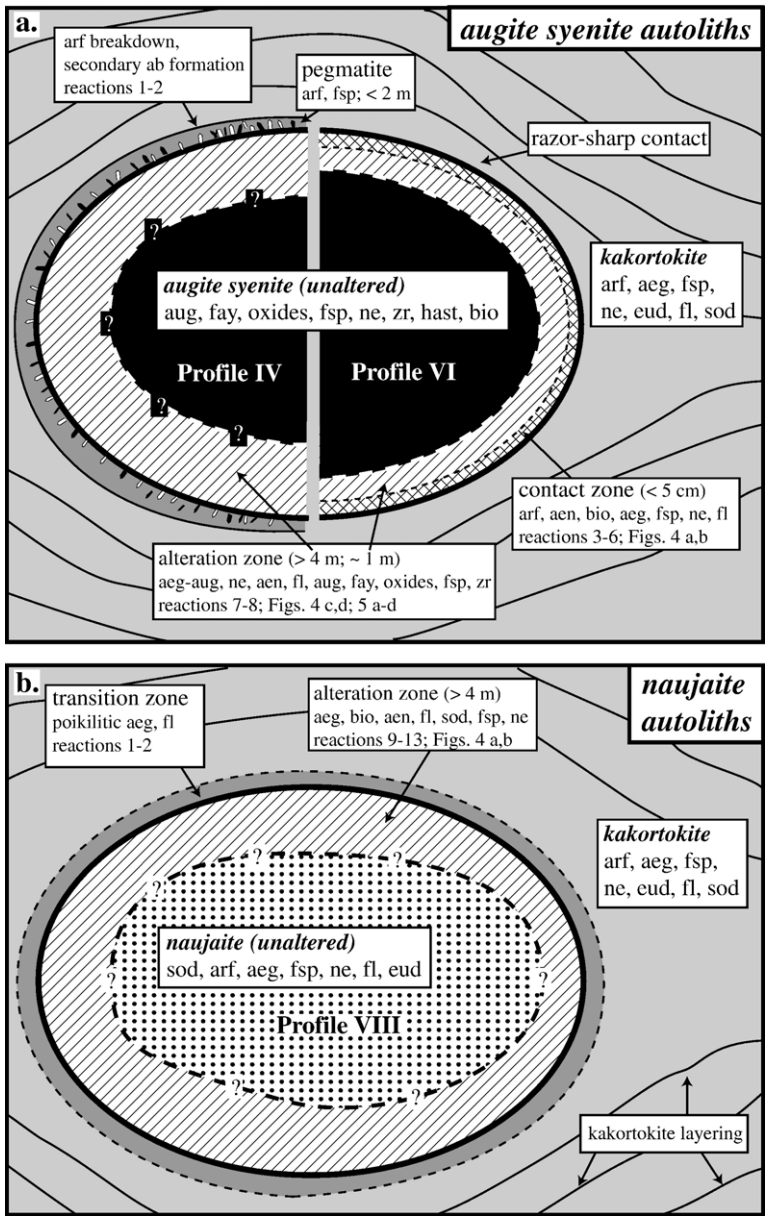

Fig. 6. (a) Schematic sketch of an augite syenite autolith in the layered kakortokite. The observed interaction textures are indicated. The left side of the autolith represents the alterations in profile IV with a border pegmatite, whereas the right side shows the alterations of profile VI with a razor-sharp contact. Reaction numbers are listed in Table 2 and explained in the text. (b) Schematic sketch of an altered naujaite autolith in the kakortokite. Note that the thickness of the alteration zones in both figures is not to scale. The diameter of the autoliths reaches up to 700 m (cf. Fig. 1). Mineral abbreviations: arf: arfvedsonite, ab: albite, fsp: feldspar, aeg: aegirine, ne: nepheline, eud: eudialyte, fl: fluorite, sod: sodalite, aug: augite, fay: fayalite, zr: zircon, hast: hastingsite, bio: biotite, aen: aenigmatite.

The raw data were corrected by an internal $\phi\rho Z$ correction (Armstrong, 1991). Analytical uncertainties are below 1% relative for major elements reaching up to 5% relative for minor elements.

The primary mineral compositions of all rock types were investigated by other authors (e.g. Larsen, 1976, 1977, 1981; Markl et al., 2001; Marks and Markl, 2001; Marks et al., 2004). Therefore, we focus on minerals from the reaction textures. Unless indicated differently, sample XL55 refers to the augite syenitic part of it. Tables with representative microprobe analyzes of the mineral

phases can be found in the online repository (see Appendix A).

4.2. Amphibole

Amphiboles in *augite syenites* are Ca and Al-rich hastingsites and subordinate ferro-edenites and katophorites (after Leake, 1997; Fig. 7a). Ti contents reach up to 0.40 pfu. Amphiboles of sample XL55, the *kakortokites* and *naujaites* are arfvedsonites and ferric-ferronyböites. They have Ti contents of <0.15 pfu in XL55 and <0.12 pfu in kakortokites and naujaites. Fluorine contents reach up to 0.82 wt.%. In augite syenites, F contents decrease with increasing X_{Fe} (Fe^{2+}/(Fe^{2+} Mg)); Fig. 7b). In contrast to the augite syenites ($0.55<X_{Fe}<0.99$), X_{Fe} of kakortokites and naujaites is nearly constant ($X_{Fe}=0.95–0.98$) without any correlation with fluorine. Amphiboles in sample XL55 have either $X_{Fe}<0.8$ and F contents above 0.2 pfu or $X_{Fe}>0.9$ and F contents below 0.2 pfu (Fig. 7b).

4.3. Clinopyroxene

In the *augite syenites*, type 1 clinopyroxene is primary augite (Quad >85 mol%, aegirine <14 mol%, jadeite ≤4 mol%). Type 2 pyroxenes (64–96 mol%

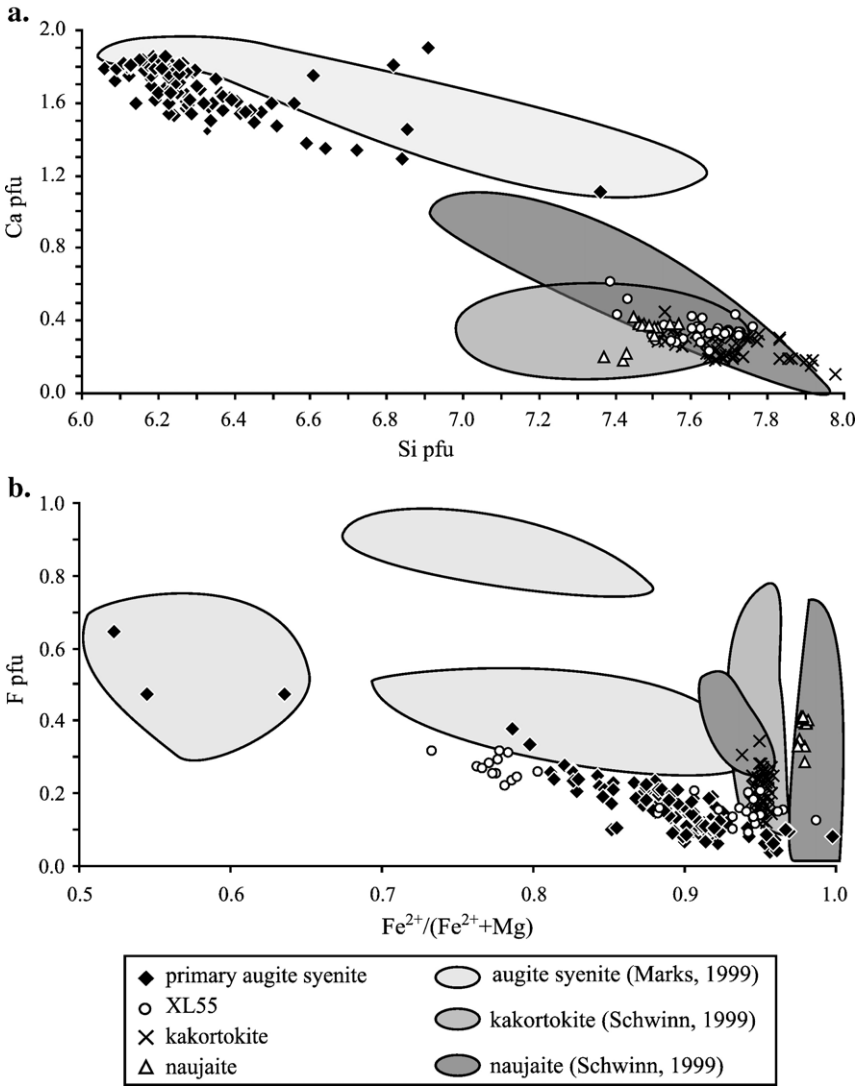

Fig. 7. (a) Amphibole classification diagram (Mitchell, 1990) for the different rock types. (b) Compositional dependence of F vs. Fe in amphiboles from the different rock types. Data from Marks (1999) and Schwinn (1999).

Quad, 4–35 mol% aegirine, 0–10 mol% jadeite; Fig. 8) are decomposition products of primary amphibole. Type 2 pyroxenes show an increase in Na and Fe^{3+} towards the autolith–kakortokite contact (Fig. 9). Additionally, type 1 pyroxenes have slightly higher TiO_2 contents (<0.98 wt.%) than type 2 (<0.3 wt.%). Pyroxenes from sample XL55 have high aegirine contents (58–86 mol %), 2–7 mol% jadeite and 10–39 mol% Quad content. The TiO_2 content of XL55 pyroxenes ranges between 0.1 and 0.9 wt.%. Their composition is similar to the pyroxenes of the kakortokites.

Clinopyroxenes in *kakortokites* and *naujaites* are almost end-member aegirines (Fig. 8). Aegirines of the kakortokites incorporate between 0.33 and 1.65 wt.% TiO_2. In the naujaites, two types can be distinguished. Type 1 is related to amphibole breakdown and has low TiO_2 contents (<1 wt.%). Type 2 formed by decomposition of aenigmatite and has TiO_2 contents of up to 4.19 wt.%.

4.4. Aenigmatite

Aenigmatites are mainly characterized by an exchange of $NaSi \rightarrow CaAl$ (rhoenite, Fig. 10a–c) and $Fe^{2+}Ti \rightarrow 2\,Fe^{3+}$ (wilkinsonite, Fig. 10a; Kunzmann, 1999). Aenigmatites in *kakortokites* (kakortokitic part of XL55) show high aenigmatite contents (78–89 mol%), 10–21 mol% wilkinsonite and <1 mol% rhoenite contents (Fig. 10). They exhibit the highest Na contents of all analyses (>2.10 pfu). These higher than in the stoichiometric Na-contents are probably due to analytical difficulties (Larsen, 1977).

Aenigmatites in XL55 have a rhoenite component of <5 mol% and a Na content between 1.9 and 2.1 pfu. Aenigmatites from the other *augite syenites* display a significant enrichment in the rhoenite component (<22.7 mol%) and a decrease in the aenigmatite component (Fig. 10a–b) with increasing distance from the contact.

Aenigmatite in *naujaites* has low rhoenite (<2 mol%) and high aenigmatite contents (up to 94 mol%).

4.5. Olivine

Olivine compositions in the *augite syenites* range from $Fa_{86}Fo_9Te_4$ to $Fa_{91}Fo_3Te_6$ and agree well with Marks and Markl (2001).

4.6. Biotite

All biotites have X_{Fe} between 0.78 and 0.99. The TiO_2 content of biotites in the *augite syenite* ranges between 1.79 and 5.76 wt.% (=0.12–0.36 pfu), while it is lower (0.72–2.34 wt.%) in sample XL55.

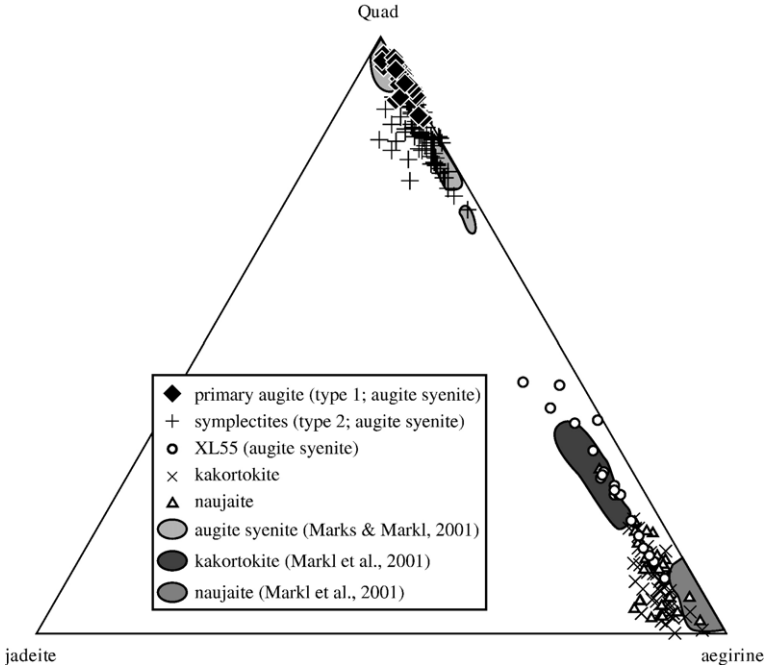

Fig. 8. Pyroxene classification in the Aegirine–Jadeite–Quad triangle.

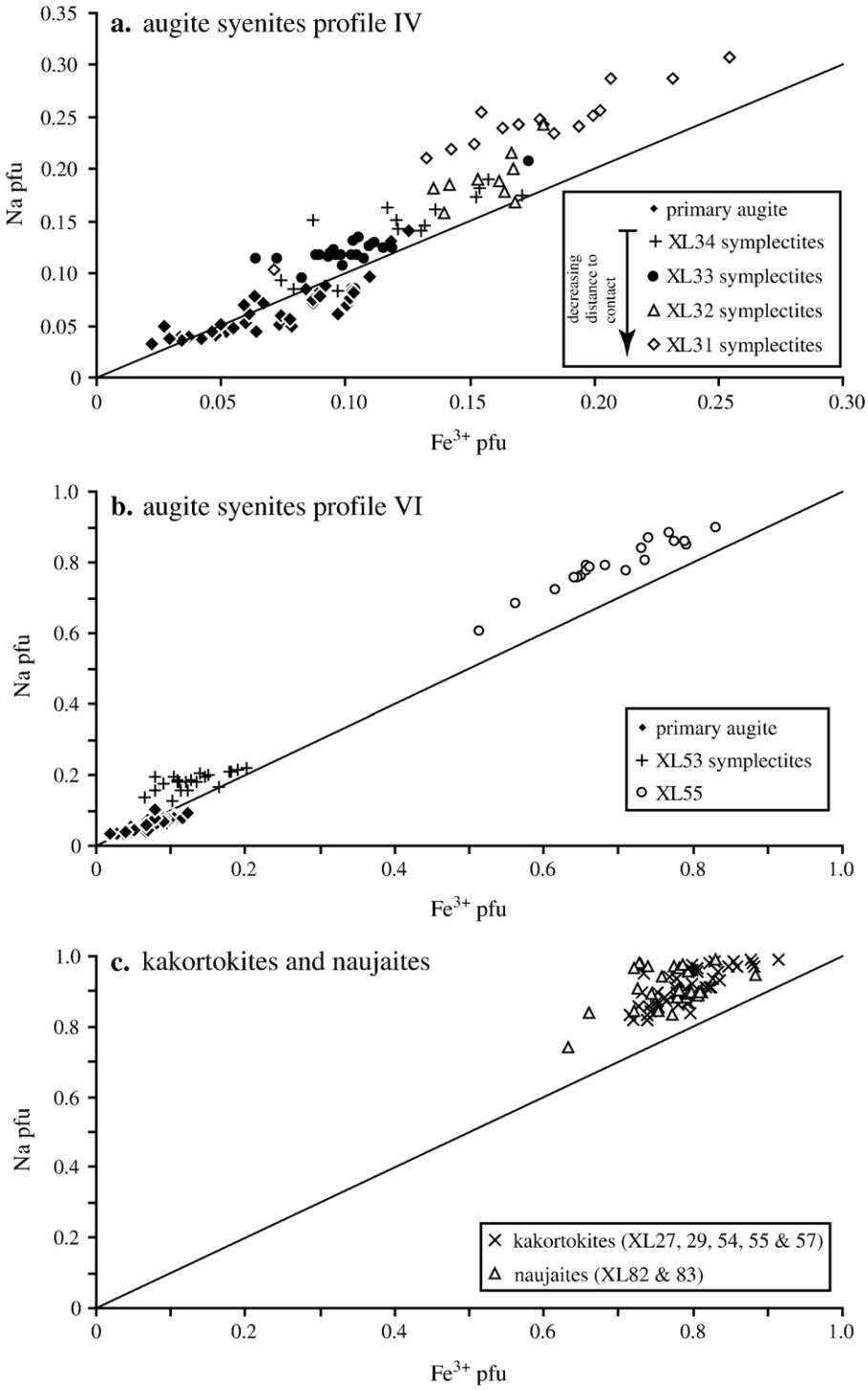

Fig. 9. Dependence of Na vs. Fe^{3+} content of the pyroxenes in the different sample suites and rock types.

Additionally, biotites in XL55 have high X_{Fe} (0.92–0.97). Some biotites in the *naujaite* deviate strongly from the theoretical biotite formula with errors in site occupancy and low totals. This error could be attributed to cations not measured, particularly Li which could originate from the decomposition of arfvedsonite.

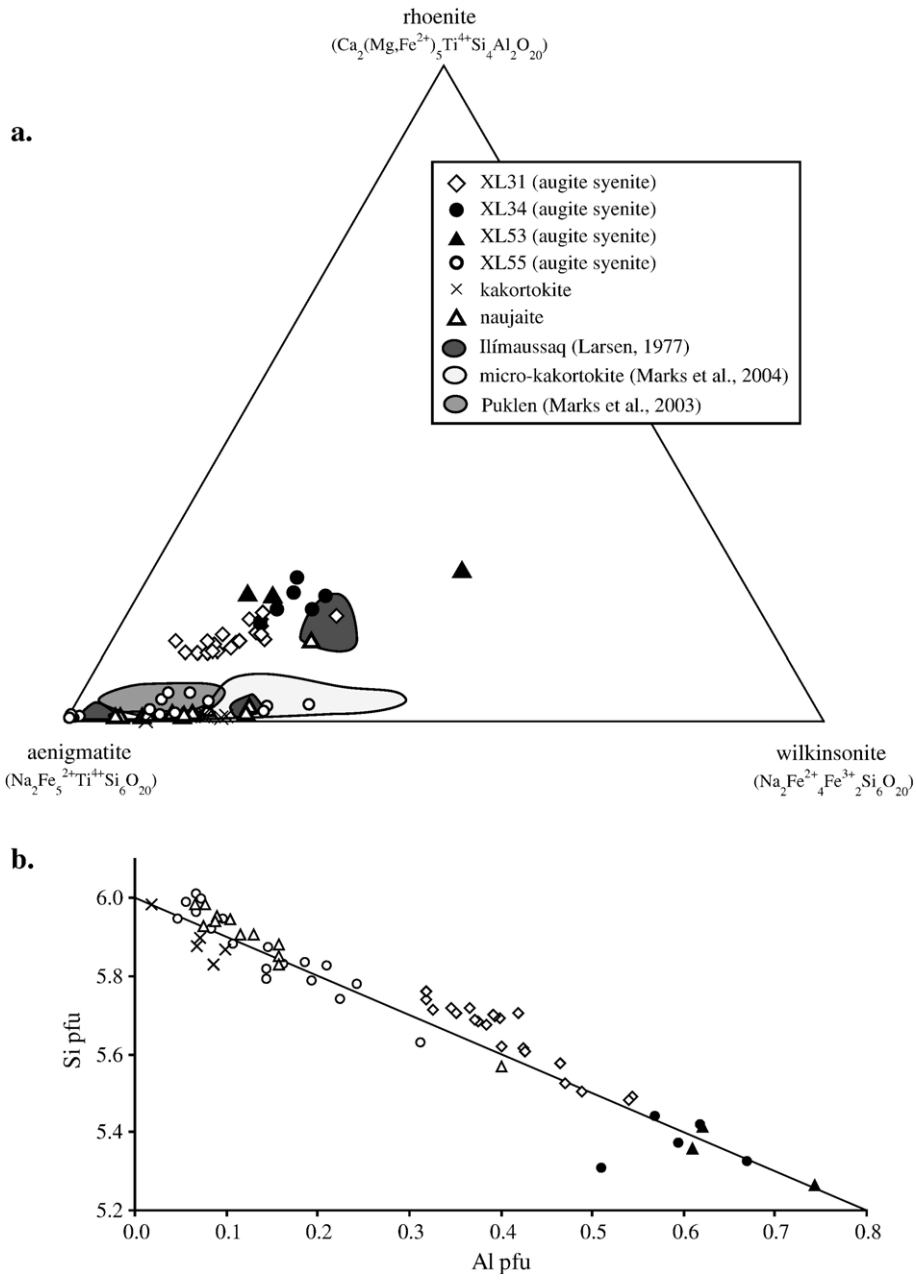

Fig. 10. (a) Rhoenite–wilkinsonite–aenigmatite classification diagram (Kunzmann, 1999) of all measured aenigmatites. (b) The mineral composition of the aenigmatites is outlined by the Si vs. Al plot. Data from Larsen (1977) and Marks et al. (2003, 2004)

4.7. Alkali feldspar

The feldspars from the *augite syenites* show ternary compositions of $Ab_{40–55}An_{6–12}Or_{33–54}$ (Larsen, 1981; Marks and Markl, 2001). Feldspar composition in the *kakortokites*, which are similar to those in the *naujaites* were recalculated by Markl et al. (2001) to $Ab_{30–45}An_{0–1}Or_{64–70}$.

4.8. Nepheline

Nephelines in the *augite syenites* can be divided into two texturally different groups: primary interstitial nephelines and secondary nephelines in reaction textures related to amphibole decomposition. Both types show very similar compositions between $Nec_{66}Qz_{18}Ks_{16}$ and $Ne_{73}Qz_8Ks_{19}$. Primary nephelines of the unaltered

sample XL50 with no secondary fluorite grains have CaO contents up to 0.7 wt.%, whereas nepheline grains surrounded by secondary fluorite have CaO contents <0.15 wt.%. Secondary nephelines in the augite syenites developed in reaction textures usually have CaO contents <0.35 wt.%.

5. Discussion

The fact that autoliths of sodalite-rich flotation cumulates (naujaite) occur below their original crystallization position must indicate variations in melt density during crystallization. According to Larsen and Sørensen (1987), the agpaitic melt, which crystallized the kakortokites and naujaites had a density of around 2.29 g/cm^3, which is identical to the density of sodalite (2.27–2.33 g/cm^3 according to Deer et al., 2004). Larsen and Sørensen (1987) calculated melt densities of >2.29 g/cm^3 at 900 °C and 1 kbar allowing sodalite to float upwards, adding 4.20 wt.% water to the composition of a dike rock which represent the initial magma composition of the Ilímaussaq agpaites. The interstitial minerals of the naujaite (arfvedsonite, feldspar, nepheline, eudialyte, fluorite etc.) crystallized from "trapped" residual melts.

The roof collapse responsible for autolith formation happened after the crystallization of large parts of the magma chamber (i.e. naujaites and kakortokite layers −11 to +2). Late agpaitic melts are enriched in volatile elements like F or H_2O, which lower the melt's density (e.g. Lange and Carmichael, 1990), because they do not exsolve a separate fluid phase (Sood and Edgar, 1970). Accordingly, these late melts had densities sufficiently low to allow the naujaites to sink.

The assumption that the observed reaction textures were related to the sinking of the autoliths into the partly crystallized kakortokite magma is supported by the fact that most of these reaction textures are exclusively found in the autoliths and not in the non-autolithic rocks. Based on field observations and petrography, there is no evidence of any chemical interaction of melt with the studied autoliths. Hence, we believe that a fluid phase released from the partly solidified kakortokites accounts for the alteration textures.

5.1. Interpretation of the observed mineral reactions related to the interaction of the autoliths and a fluid phase

5.1.1. Reactions in the kakortokites

In kakortokite samples close to the contact with the autoliths, primary arfvedsonitic amphibole is replaced by aegirine (XL29, 77 and 78):

$$\text{arfvedsonite} + O_2 + 2\ Na^+ + 2\ SiO_2^{(fluid)} \rightarrow 5\ \text{aegirine} + 2\ H^+ \quad (1)$$

The fluorine released from the arfvedsonites is conserved close to the reaction site forming fluorite with Ca either from the arfvedsonite or from the fluid phase:

$$Ca^{2+} + 2\ F^- \rightarrow \text{fluorite}. \quad (2)$$

5.1.2. Reactions in the augite syenite autoliths

5.1.2.1. Reactions close to the contact

Formation of biotite. Biotite in sample XL55 probably formed during decomposition of primary olivine according to the following reaction:

$$3\ \text{fayalite} + 2\ \text{orthoclase} + 2\ H_2O \rightarrow 2\ \text{annite} + SiO_2^{(fluid)}. \quad (3)$$

However, the analyzed biotites contain up to 2.34 wt.% TiO_2, which indicates that Fe–Ti oxides must have participated in this reaction.

Formation of aenigmatite. Aenigmatite formed at the expense of Fe–Ti oxides (Fig. 4b):

$$\text{ulvøspinel} + 2\ Na^+ + 3\ Fe^{2+} + 6\ SiO_2^{(fluid)} + 4\ H_2O \rightarrow \text{aenigmatite} + 8\ H^+ \quad (4)$$

Formation of arfvedsonite. Arfvedsonite is the dominant mafic mineral phase close to the contact (Fig. 4a). Its chemical composition and abundance suggests that it formed by complete replacement of primary pyroxene (see Section 5.2.1.):

$$\text{pyroxene} + \text{fluidA} \rightarrow \text{amphibole} + \text{fluidB} \quad (5)$$

Formation of fluorite. Fluorite commonly occurs as inclusions in arfvedsonite (Fig. 4a). It formed by reaction of Ca released during pyroxene breakdown with fluorine from the fluid. Furthermore, fluorite grains are common at grain boundaries of nepheline and alkali feldspar (see below).

Formation of pyroxene. The rims of small secondary arfvedsonite grains are commonly replaced by aegirine (Fig. 4b) and nepheline:

$$\text{arfvedsonite} + O_2 + \text{albite} + 2\ Na^+ \rightarrow 5\ \text{aegirine} + \text{nepheline} + 2\ H^+ \quad (6)$$

5.1.2.2. Reactions far from the contact

Amphibole decomposition. The most frequently observed reaction within the augite syenite autoliths is the decomposition of hastingsite to two-phase and three-phase symplectites (Fig. 5a–d). The following schematic reaction may describe this (see Section 5.2.2. for detailed discussion):

$$\text{amphibole} + \text{fluid A} \rightarrow \text{pyroxene} + \text{nepheline} \pm \text{aenigmatite} + \text{fluid B} \quad (7)$$

The presence or absence of aenigmatite in the reaction products cannot be related to the composition of the precursor amphibole, as they have rather constant TiO_2 contents which probably govern the formation of aenigmatite. Hence, Ti must have been mobile in some but not all symplectites. This might be due to locally variable pH or F concentrations of the fluid phase resulting in a variable transport capacity for Ti (e.g. Van Baalen, 1993; Rubin et al., 1993; Salvi et al., 2000).

Fluorite formation. Small fluorite grains are concentrated along grain boundaries of interstitial (primary) nepheline (Fig. 4c and d). It is therefore assumed that Ca from nepheline reacted with fluorine from the fluid circulating through the augite syenites:

$$Ca_{0.5}AlSiO_4(\text{nepheline}) + Na^+ + F^- \rightarrow \text{fluorite} + \text{nepheline} \quad (8)$$

The elevated Ca content in unaltered nephelines support this hypothesis (Section 4.8).

5.1.3. Reactions in the naujaite autoliths

Formation of aegirine–biotite intergrowths. Arfvedsonite exhibits reaction textures consisting of pyroxene–biotite intergrowths (Fig. 5e, see Section 5.2.3. for quantification):

$$\text{arfvedsonite} + \text{fluid A} \rightarrow \text{aegirine} + \text{biotite} + \text{fluid B} \quad (9)$$

The contact between the amphibole or the product intergrowths and the adjacent sodalite is sharp and probably reflects the former grain boundaries (Fig. 5e).

Fluorite formation. In the naujaites, the same fluorite-forming reactions apply as mentioned for the kakortokites and augite syenites.

Aenigmatite formation. Aenigmatite is very common in the altered naujaite samples. According to Marks and Markl (2003), two reactions could be responsible for the aenigmatite formation:

$$4\ \text{arfvedsonite} + 2\ Na^+ + 2\ Ti^{4+} + H_2O + 1.5\ O_2 \rightarrow 10\ \text{aegirine} + 2\ \text{aenigmatite} + 10\ H^+ \quad (10)$$

$$10\ \text{aegirine} + 2\ Ti^{4+} + H_2O \rightarrow \text{aenigmatite} + 2.5\ O_2 + 6\ Na^+ + 8\ SiO_2^{(\text{fluid})} + 2\ H^+ \quad (11)$$

Ti can be balanced by its incorporation into the reactants arfvedsonite and aegirine. Petrography does not allow to decide between the two possibilities.

Aenigmatite decomposition. As a late stage phenomenon in the naujaites, aenigmatite decomposes to Ti-rich aegirine (<4.19 wt.% TiO_2) and Fe–Ti oxides (Fig. 5f, cf. Larsen, 1977):

$$2\ \text{aenigmatite} + 2\ Na^+ + 1.5\ O_2 + H_2O \rightarrow 2\ \text{ulvøspinel} + 6\ \text{aegirine} + 2\ H^+. \quad (12)$$

Biotite grains occur at grain boundaries of aenigmatite and aegirine (+Fe–Ti oxides). As most reactions involving pyroxenes are redox reactions (e.g., reactions (1), (6) and (10)), the formation of biotite from aenigmatite seems more likely than from aegirine, which would be a reduction reaction:

$$3\ \text{aenigmatite} + 3\ \text{orthoclase} + 6\ H^+ \rightarrow 3\ \text{biotite} + 3\ \text{ulvøspinel} + 19\ SiO_2 + 6\ Na^+ \quad (13)$$

5.2. Balanced mineral reactions

In order to understand the fluid–autolith mineral reactions detailed above and in Table 2, we quantified the following four typical representatives applying either the isocon method (Grant, 1986) or assuming constant volume:

- The formation of arfvedsonite at the expense of pyroxene in the augite syenites (reaction (5)).
- The formation of pyroxene–nepheline (two-phase symplectites) pyroxene–nepheline–aenigmatite (three-phase symplectites) by amphibole decomposition in the augite syenites (reaction (7)).
- The formation of pyroxene–biotite intergrowths by decomposition of amphibole in the naujaites (reaction (9)).

Whereas reaction (9) shows textural evidence of volume conservation (Fig. 5e), textures of reactions (5) and (7) (Figs. 4a/b, 5a–d) imply that they occurred in an

Table 2
Mineral-reactions in the kakortokites, augite syenites and naujaites

Reactions within the enveloping kakortokites			
(1)	arfvedsonite + O_2 + 2 Na^+ + 2 SiO_2	→	5 aegirine + 2 H^+
(2)	Ca^{2+} 2 F^-	→	Fluorite
Reactions within the augite syenite autoliths			
Close to the contact			
(3)	3 fayalite + 2 orthoclase + 2 H_2O	→	2 annite + SiO_2
(4)	ulvøspinel + 2 Na^+ 3 Fe^{2+} 6 SiO_2 + 4 H_2O	→	aenigmatite + 8 H^+
(5)	pyroxene + fluid A	→	amphibole + fluid B
(6)	arfvedsonite + O_2 + albite + 2 Na^+	→	5 aegirine + nepheline + 2 H^+
Up to several meters inside the autoliths			
(7)	amphibole + fluid A	→	pyroxene + nepheline ± aenigmatite + fluid B
(8)	$Ca_{0.5}AlSiO_4$ (nepheline) + Na^+F^-	→	fluorite + nepheline
Reactions within the naujaite autoliths			
(9)	arfvedsonite + fluid A	→	aegirine + biotite + fluid B
(10)	4 arfvedsonite + 2 Na^+ 2 Ti^{4+} 1.5 O_2 + H_2O	→	10 aegirine + 2 aenigmatite + 10 H^+
(11)	10 aegirine + 2 Ti^{4+} H_2O	→	aenigmatite + 2.5 O_2 + 6 Na^+ 8 SiO_2 + 2 H^+
(12)	2 aenigmatite + 2 Na^+ 1.5 O_2 + H_2O	→	2 ulvøspinel + 6 aegirine + 2 H^+
(13)	3 aenigmatite + 3 orthoclase + 6 H^+	→	3 biotite + 3 ulvøspinel + 19 SiO_2 + 6 Na^+

open system where neither isochemical conditions nor constant volume can be assumed. We used the calculation scheme outlined by NiWen et al. (1991) and Wagner and Cook (1997) based on the isocon method of Grant (1986). First, mean compositions of each mineral phase involved were recalculated to a common anion-basis (O + F + Cl). If more than one product phase was present, the required volume proportions of the product phases were determined by the ICW image analysis of the electron microprobe, because the two-dimensional proportions closely approximate their true volume proportions. We assigned an overall error of about 10–15% to the determination of volume proportions, which accounts for most of the total error of the entire calculation procedure. Subsequently, these data were corrected for density differences using unit-cell dimensions and unit-cell volumes taken from Kelsey and McKie (1964), Nolan (1969), Hawthorne (1976), Harlow (1982), Makino and Tomita (1989) and Hovis et al. (1992). The atomic concentrations of the reactant and the bulk product (symplectite) were plotted in an isocon diagram (Fig. 11). The isocon was determined graphically as a best fit straight line through the origin, defined by immobile elements. The slope was then used to calculate the reaction stoichiometry according to NiWen et al. (1991).

5.2.1. Pyroxene breakdown in the augite syenite autoliths close to the contact (reaction (5))

We chose Si, Al and Mn as isocon-defining elements as this option is most consistent with the geochemical constraints (Fig. 11a, left side) for the quantification of reaction (5). Most of the elements lie very close to the isocon line (Fig. 11a, left side; gain and loss diagram Fig. 11a, right). Volume data and mean compositions of the involved clinopyroxene and amphibole are given in Table 3. The reaction was calculated as:

$$4.00\ \text{pyroxene} + 2.06\ Na^+ + 0.46\ K^+ + 0.52\ Fe^{3+} + 0.54\ Fe^{2+} + 0.02\ Ti^{4+} + 0.01\ Al^{3+} + 0.28\ F^- + 2.00\ H^+ \rightarrow 1.01\ \text{amphibole} + 0.01\ Mn^{2+} + 0.30\ Mg^{2+} + 3.20\ Ca^{2+} + 0.14\ H_2O \quad (5a)$$

Hence Na, H, Fe, K and F were added and Ca and little Mg were released. Note that the H_2O on the product side of reaction (5a) was required for the charge balance. The formation of secondary amphibole is characterized by no significant mass change (−1%) whereas the volume increased by about 11%.

The secondary arfvedsonites contain abundant inclusions of fluorite (Fig. 4a). A complete retention of the Ca released during pyroxene breakdown would require an amphibole and fluorite volume proportion of about 79 and 21 vol.%, which is in excellent agreement with the measured volume proportions of 81–84 and 16–19 vol. %, respectively. Hence, the released Ca was immediately consumed by the formation of fluorite.

5.2.2. Amphibole breakdown in the augite syenite autoliths (reaction (7))

The most common reaction is the breakdown of amphibole to two- and three-phase symplectites

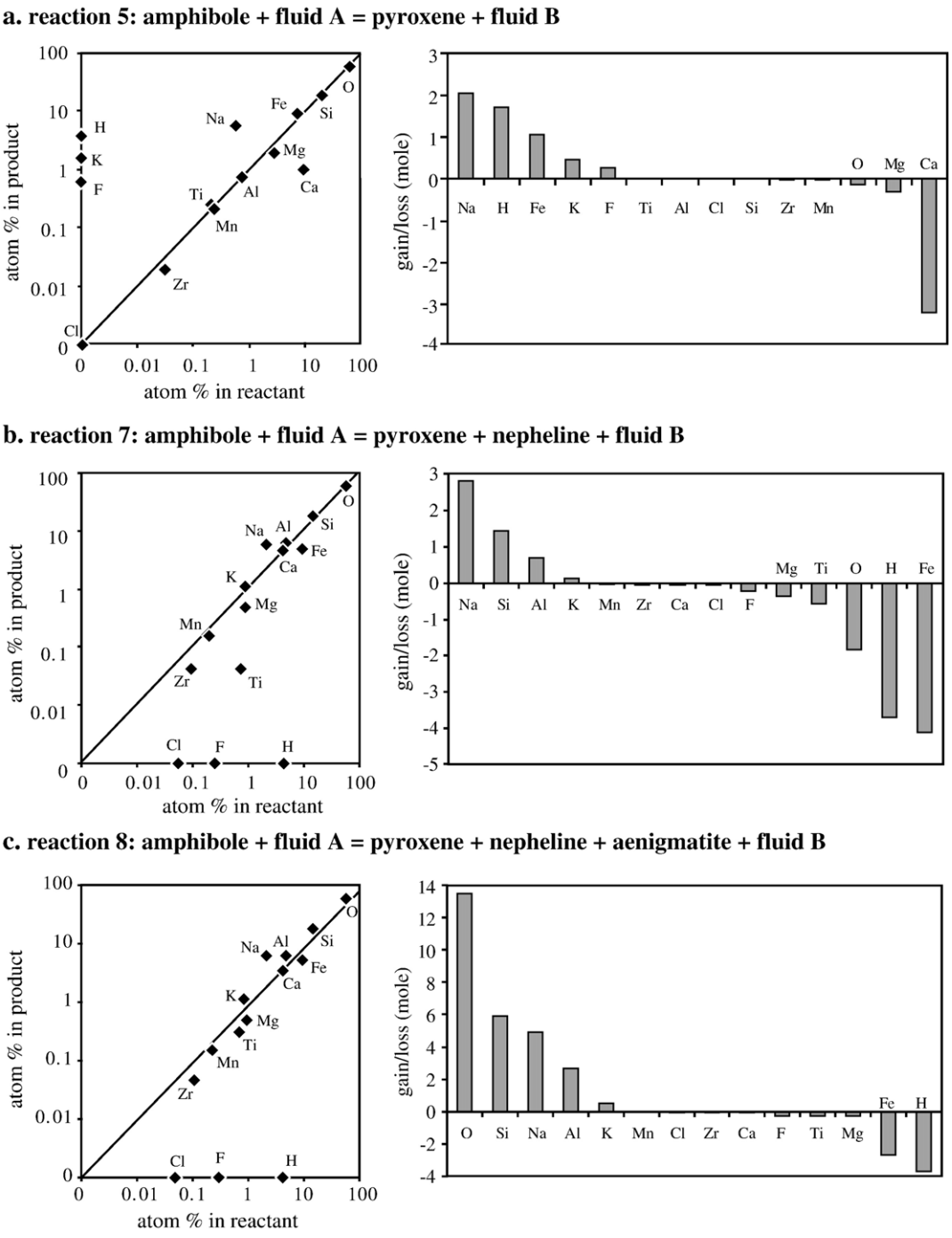

Fig. 11. Isocon diagrams (left side) of reactions (5), (7a) and (7c) with add-and loss-diagrams (right side). See text for discussion.

(reaction (7)). We chose Ca and Mn for the definition of the isocon, the Ca content being most influential for the slope of the isocon. This choice appears reasonable, because we observed no fluorite formation close to the reaction texture. If there had been an intergranular fluid phase that was compositionally similar to the one involved in pyroxene breakdown (reaction (5)), any Ca released would have immediately resulted in fluorite precipitation.

The volume proportions for the different reaction textures vary considerably. The two-phase symplectites range from 40 to 55 vol.% pyroxene and 60–45 vol.%

Table 3
Volume data and mean composition of mineral phases involved in reactions (5) and (7)

Reaction no.	(5)			(7a)			(7c)			
	cpx	amph		amph	cpx	ne	amph	cpx	ne	aen
Vol.% in intergrowth		100			51	49		40	51	9
Vol per 24 anions (Å^3)	449.0	447.0	48 anions (Å^3)	940.1	897.9	1088.1	940.1	897.9	1088.1	893.4
% in intergrowth					56	44		44	46	10
Formulae			Formulae							
Si	1.94	7.70	Si	6.22	1.98	1.07	6.20	2.01	1.08	5.72
Ti	0.02	0.10	Ti	0.31	0.01	0.00	0.29	0.01	0.00	0.90
Al	0.07	0.31	Al	2.03	0.06	0.92	2.00	0.04	0.90	0.37
Fe (total)	0.70	3.83	Fe (total)	3.93	0.85	0.01	3.95	0.82	0.02	4.67
Fe^{2+}	0.63	3.03	Fe^{2+}	3.88	0.69	0.00	3.74	0.68	0.00	4.45
Fe^{3+}	0.07	0.80	Fe^{3+}	0.05	0.16	0.02	0.21	0.14	0.02	0.23
Mn	0.02	0.09	Mn	0.08	0.03	0.00	0.09	0.03	0.00	0.13
Mg	0.28	0.81	Mg	0.37	0.09	0.00	0.38	0.10	0.00	0.13
Ca	0.90	0.41	Ca	1.79	0.80	0.00	1.78	0.75	0.01	0.21
Na	0.06	2.28	Na	0.86	0.19	0.73	0.91	0.23	0.73	1.86
K	0.00	0.45	K	0.36	0.00	0.17	0.35	0.00	0.17	0.00
Zr	0.00	0.01	Zr	0.04	0.00	0.00	0.04	0.01	0.00	0.01
Cl	0.00	0.00	Cl	0.02	0.00	0.00	0.02	0.00	0.00	0.00
F	0.00	0.28	F	0.11	0.00	0.00	0.13	0.00	0.00	0.00
O	6.00	23.72	O	23.86	6.00	4.00	23.85	6.00	4.00	20.00
H	0.00	1.71	H	1.85	0.00	0.00	1.84	0.00	0.00	0.00

nepheline. The three-phase symplectites show variations of 32–51 vol.% pyroxene, 39–55 vol.% nepheline and 9–13 vol.% aenigmatite. We present calculations for volume proportions of 51 vol.% pyroxene and 49 vol.% nepheline and of 40 vol.% pyroxene, 51 vol.% nepheline and 9 vol.% aenigmatite, respectively. Volume data for the reactions and mean compositions of the mineral phases involved are given in Table 3. The two-phase symplectites formed according to (Fig. 11b):

$$\begin{aligned}2.00\ \text{amphibole} &+ 1.43\ SiO_2 + 0.69\ Al^{3+} + 2.82\ Na^+ \\ &+ 0.12\ K^+ + 0.17\ O_2 + 6.46\ H^+ \\ \rightarrow &4.27\ \text{pyroxene} + 5.07\ \text{nepheline} + 0.58\ Ti^{4+} \\ &+ 4.12\ Fe^{2+} + 0.37\ Mg^{2+} + 0.04\ Mn^{2+} \\ &+ 0.05\ Ca^{2+} + 0.04\ Zr^{4+} + 0.05\ Cl^- + 0.23\ F^- \\ &+ 5.08\ H_2O \end{aligned} \quad (7a)$$

Considering that Si, Al, Na and K were added during this reaction, we assume that feldspar from the surrounding augite syenite matrix was involved in the reaction. The exact volume proportion of the feldspar involved is unknown. Therefore, we used Al, which is the most immobile of these four elements, to determine the quantity of feldspar consumed in the reaction. Assuming that all of the K was also derived from the feldspar because the fluid phase is definitely Na-rich (the added Na in reactions (7a) and (5a)), we chose a reasonable feldspar composition of $Ab_{0.83}Or_{0.17}$ to recalculate the reaction. The result should be considered as estimate:

$$\begin{aligned}2.00\ \text{amphibole} &+ 0.69\ \text{feldspar} + 2.25\ Na^+ \\ &+ 0.17\ O_2 + 9.22\ H^+ \\ \rightarrow &4.27\ \text{pyroxene} + 5.07\ \text{nepheline} + 0.58\ Ti^{4+} \\ &+ 4.12\ Fe^{2+} + 0.37\ Mg^{2+} + 0.64\ SiO_2 \\ &+ 0.04\ Mn^{2+} + 0.05\ Ca^{2+} + 0.04\ Zr^{4+} \\ &+ 0.05\ Cl^- + 0.23\ F^- + 6.46\ H_2O \end{aligned} \quad (7b)$$

The three-phase symplectite formed according to (Fig. 11c):

$$\begin{aligned}2.00\ \text{amphibole} &+ 5.92\ SiO_2 + 2.65\ Al^{3+} + 4.91\ Na^+ \\ &+ 0.51\ K^+ + 0.11\ O_2 + 1.40\ H_2O \\ \rightarrow &4.47\ \text{pyroxene} + 7.06\ \text{nepheline} \\ &+ 0.30\ \text{aenigmatite} + 0.26\ Ti^{4+} + 0.26\ Mg^{2+} \\ &+ 0.03\ Mn^{2+} + 0.06\ Ca^{2+} + 2.67\ Fe^{2+} \\ &+ 0.04\ Zr^{4+} + 0.04\ Cl^- + 0.25\ F^- + 6.48\ H^+ \end{aligned} \quad (7c)$$

This reaction, recalculated with a feldspar composition of $Ab_{0.81}Or_{0.19}$, reads as:

$$\begin{aligned}2.00\ \text{amphibole} + 2.65\ \text{feldspar} + 2.74\ Na^{+} \\ + 0.11\ O_2 + 4.12\ H^{+} \\ \rightarrow 4.47\ \text{pyroxene} + 7.06\ \text{nepheline} \\ + 0.30\ \text{aenigmatite} + 0.26\ Ti^{4+} + 0.26\ Mg^{2+} \\ + 2.03\ SiO_2 + 0.03\ Mn^{2+} + 0.06\ Ca^{2+} \\ + 2.67\ Fe^{2+} + 0.04\ Zr^{4+} + 0.04\ Cl^{-} + 0.25\ F^{-} \\ + 3.90\ H_2O \qquad (7d)\end{aligned}$$

Both reactions show a similar addition of Na whereas Fe, Mg, F and (overall) H were released. H^+ and H_2O were introduced for charge balance. Note, that Ti is highly mobile in reaction (7a)/(7b). The mass (ΔM) and volume (ΔV) changes for reactions (7b) and (7d) as −17% and −11%, and −11% and −10% respectively.

5.2.3. Amphibole breakdown in the naujaite autolith (reaction (9), constant volume)

The amphibole breakdown in the naujaites (reaction (9)) shows textural evidence of volume conservation. The volume proportions of the aegirine biotite intergrowths range from 70/30 to 66/34. The quantification refers to average volume proportions of 68/32:

$$\begin{aligned}2.00\ \text{amphibole} + 0.44\ SiO_2 + 0.08\ Mn^{2+} \\ + 0.03\ Mg^{2+} + 0.03\ Ca^{2+} + 0.17\ Na^{+} \\ + 0.39\ K^{+} + 0.01\ Zr^{4+} + 0.60\ O_2 + 0.18\ H_2O \\ \rightarrow 5.87\ \text{pyroxene} + 1.16\ \text{biotite} + 0.11\ Fe^{2+} \\ + 0.04\ Ti^{4+} + 0.06\ Al^{3+} + 0.76\ F^{-} + 1.18\ H^{+} \\ (9a)\end{aligned}$$

Besides an addition of O, K, Si and the release of the volatile elements F and H, there is no significant change of elements. In contrast to the reactions in the augite syenite autoliths, Na and Fe remain virtually unchanged during this alteration. The released F and H were probably retained in the autoliths to form the commonly observed fluorite and alteration products of sodalite (analcime and natrolite). There is a small mass increase of about 2.5% during this reaction.

5.3. Estimation of equilibration temperatures and relative oxygen fugacity during fluid–autolith interaction

QUILF calculations (Andersen et al., 1993; Marks and Markl, 2001) with coexisting olivines and clinopyroxenes of augite syenite samples XL 32, 33, 34, 50 and 53 gave a temperature range between 640 and 770 °C. The sample in which no alteration textures were observed (XL50) showed the highest temperatures of 723–770 °C. These temperatures are interpreted to reflect reequilibration during autolith entrapment into the kakortokitic magma.

It is reasonable to assume that the fluid–autolith reactions took place during further cooling after the autolith-forming event. The oxygen fugacity and the temperatures of the autoliths' entrapment can be estimated by comparing the stability of mafic minerals (in particular hastingsite, aenigmatite and arfvedsonite; Nicholls and Carmichael, 1969; Thomas, 1982; Fig. 12) with the T-f_{O2} crystallization path of the Ilímaussaq complex (Markl et al., 2001). The decomposition of arfvedsonite in the kakortokite, augite syenite and naujaite (reactions (1), (6) and (9)) and the aenigmatite breakdown (reactions (12) and (13)) in the naujaite autolith record continuous reactions occurring at successively higher oxygen fugacities and/or lower temperatures. Accordingly, the reactions in the autoliths (and in the kakortokite) must have taken place at temperatures below about 620 °C and at oxygen fugacities of 1–4 log units above the FMQ buffer curve (Fig. 12).

5.4. Fluid infiltration and element mobilities

In profile IV, a pegmatite is developed between the kakortokite and the augite syenite autolith. All augite syenite samples from this sample suite show alteration textures (up to 3.5 m from the contact, reactions (7) and (8)). However, profile VI (without contact pegmatite) displays only minor alteration of the augite syenite autolith (XL53, alterations are evident up to 10 cm from the contact, very subordinate in sample XL51). The fluid circulation/infiltration in the autoliths seems to be elevated where a contact pegmatite is developed and to be reduced where no pegmatite exists (Fig. 6). Furthermore, not only the presence but also the intensity of alteration in the autoliths increases with approaching the contact. For example, in the augite syenitic part of sample XL55, the mafic mineralogy is completely altered. In XL53 (10 cm from the contact), only amphiboles show decomposition textures. The same applies to the naujaite autolith (profile VIII). We suggest that the reactions were controlled by a fluid phase which circulated through the autoliths. Grain boundaries acted thereby as fluid pathways.

The fluid infiltration of the autoliths is accompanied by the addition and release of certain elements. Based on the reaction textures, on the quantified reactions and the increase of Fe^{3+} in the secondary phases and the

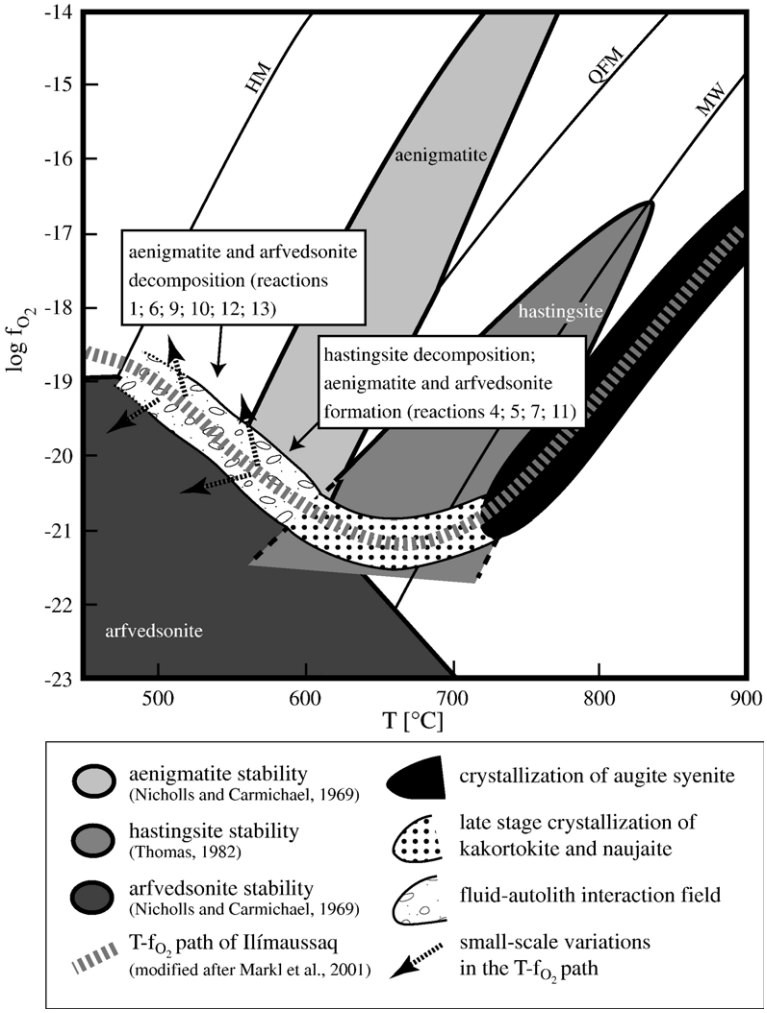

Fig. 12. Using aenigmatite, arfvedsonite (Nicholls and Carmichael, 1969) and hastingsite stability (Thomas, 1982) and the T-f_{O2} evolution of the Ilímaussaq complex slightly changed after Markl et al., 2001, the observed reactions in the augite syenite and naujaite autoliths must have taken place at temperatures below 620 °C and at f_{O2} conditions slightly above the QFM buffer. (HM hematite–magnetite buffer curve; QFM quartz–magnetite–fayalite buffer curve; MW magnetite–wüstite buffer curve).

occurrence of secondary albite and analcime, the fluid can be characterized as Na-rich and oxidizing. Several elements were released during reactions in the autoliths but are most likely conserved:

Reaction (5) (formation of secondary amphibole by pyroxene breakdown) shows a strong release of Ca that was subsequently caught up in fluorite grains. Thus, the fluid interacting with the pyroxene must have been F-rich. Inside the augite syenite autoliths, fluorine was released during amphibole breakdown (reaction (7)). In this case, fluorite could not form directly because Ca was neither released by the amphibole breakdown nor was it contained in the fluid. However, interstitial primary Ca-rich nepheline provided the Ca source required to form fluorite (reaction (8)). The chemical potential of F is higher in the kakortokite than in the augite syenite since the kakortokite precipitates magmatic fluorite. This higher chemical potential causes the infiltration of the autoliths with a F-rich fluid. It also prohibits that fluorine in the autoliths is released into the kakortokites, because the system acts to balance potential differences.

Ti shows a rather complex behavior. Amphiboles, pyroxenes and aenigmatites have different Ti contents in different textural settings. Furthermore, it seems that Ti-mobility influenced the formation of aenigmatite in the three-phase symplectites (reaction (7)). Ti is mobile in some textures and immobile in others during the late-stage replacement processes in the autoliths. Especially the amphibole decomposition to pyroxene

and nepheline (reaction (7a)/(7b)) indicates an almost complete mobility of Ti. Salvi et al. (2000 and references therein) have shown that F-rich brines can mobilize Ti and other HFSE and that fluorine forms complexes with HFSE (also Rubin et al., 1993; Van Baalen, 1993). It is important to note that a high F content in the fluid is only possible if little Ca is present. Otherwise, fluorite would form and the solubility of HFSE-bearing minerals would be lowered (Salvi et al., 2000). Together with Ti, Fe was mobilized (reaction (7)) and transferred to other parts within or expelled from the autoliths. The relocation of Fe could be evidenced by its addition in reaction (5).

6. Conclusions

- Autoliths of augite syenite and naujaite in the agpaitic kakortokites of the Ilímaussaq intrusion formed during a roof collapse and were infiltrated and altered by a Na and F-rich oxidizing fluid phase (Fig. 12). The effects of fluid metasomatism were more intensive closer to the contact of the autoliths where the augite syenite autoliths underwent replacement of the Ca–Fe^{2+}-rich mineral assemblage of augite, fayalite, Fe–Ti oxide and hastingsite by a Na–Fe^{3+}-rich assemblage of arfvedsonite, aegirine, biotite, aenigmatite and fluorite. Further from the contact, hastingsite was replaced by aegirine–augite, nepheline ± aenigmatite. Fluorite was formed at grain boundaries of primary nepheline. In the naujaite autoliths, primary arfvedsonite was replaced by aegirine and biotite and aenigmatite is very common. Close to the contact, aegirine and aenigmatite are the only mafic minerals.
- The fluid flow responsible for the reactions is mainly characterized by a one-way alteration, i.e. the fluid originated during cooling of the kakortokites and infiltrated the augite syenite and naujaite autoliths.
- The fluid–autolith interaction began at temperatures of about 620 °C with the decomposition of hastingsite and the formation of secondary aenigmatite and arfvedsonite at relative oxygen fugacities slightly above the QFM buffer. At lower temperatures and/or more oxidizing conditions, arfvedsonite and aenigmatite were replaced by aegirine ± Fe–Ti oxides. Accordingly, the interactions began during the magmatic stage (probably shortly after the roof collapse) and continued during cooling of the kakortokites. The reaction conditions are consistent with the crystallization path of the Ilímaussaq intrusion and the crystallization conditions of the kakortokites (Markl et al., 2001).
- The volatiles F and H were set free during amphibole breakdown but were locally fixed within the autoliths as fluorite or analcime. Hence, they were only relocated on the order of some mm to cm. The mobility of other elements varies. In the augite syenite autoliths, Ti was mobilized in locally varying amounts. Fe was mobilized far from the contact and added (again) close to the contact to the kakortokite. Close to the contact, Ca was the only element which was liberated in significant amounts and immediately reacted with the fluorine of the fluid to form fluorite inclusions in secondary arfvedsonite.

Acknowledgements

T. Wenzel is thanked for his help during microprobe measurements and D. Müller-Lorch for a helpful and pleasant time in the field. J. Köhler and T. Wenzel are thanked for their comments on an earlier version of this manuscript. We also thank T. Andersen and J. Bailey for constructive reviews, which helped to improve the overall quality of this work.

Appendix A. Supplementary data

Supplementary data associated with this article can be found, in the online version, at doi:10.1016/j.lithos.2006.03.024.

References

Andersen, S., Bohse, H., Steenfelt, A., 1981. A geological section through the southern part of the Ilímaussaq intrusion. Rapp.-Grønl. Geol. Unders. 103, 39–42.

Andersen, D.J., Lindsley, D.H., Davidson, P.M., 1993. QUILF; a Pascal program to assess Equilibria among Fe–Mg–Mn–Ti oxides, pyroxenes, olivine, and quartz. Comput. Geosci. 19, 1333–1350.

Armstrong, J.T., 1991. Quantitative elemental analysis of individual microparticles with electron beam instruments. In: Heinrich, K.F. J., Newbury, D.E. (Eds.), Electron Probe Quantitation. Plenum Press, New York, pp. 261–315.

Bailey, J.C., Gwozdz, R., Rose-Hansen, J., Sørensen, H., 2001. Geochemical overview of the Ilímaussaq alkaline complex, South Greenland. Geol. Greenl. Surv. Bull. 190, 32–53.

Bohse, H., Brooks, C.K., Kunzendorf, H., 1971. Field observations on the kakortokites of the Ilímaussaq intrusion, South Greenland, including mapping and analyses by portable X-ray fluorescence equipment for zirconium and niobium. Geol. Grønl. 38.

Bowden, P., 1985. The geochemistry and mineralization of alkaline ring complexes in Africa (a review). J. Afr. Earth Sci. 3, 17–39.

Deer, W.A., Howie, R.A., Zussman, J., 2004. Framework Silicates. The Geological Society London.

Drysdall, A.R., Jackson, N.J., Ramsay, C.R., Douch, C.J., Hackett, D., 1984. Rare element mineralization related to Precambrian alkali granites in the Arabian Shield. Econ. Geol. 79, 1366–1377.

Engell, J., 1973. A closed system crystal-fractionation model for the agpaitic Ilímaussaq intrusion, South Greenland, with special reference to the lujavrites. Bull. Geol. Soc. Den. 22, 276–302.

Ferguson, J., 1964. Geology of the Ilímaussaq alkaline intrusion, South Greenland. Bull.-Grønl. Geol. Unders. 39.

Ferguson, J., 1970. The significance of the kakortokite in the evolution of the Ilímaussaq intrusion, South Greenland. Bull.-Grønl. Geol. Unders. 89.

Grant, J.A., 1986. The isocon diagram — a simple solution to Gresen's equation for metasomatic alteration. Econ. Geol. 81, 1976–1982.

Harlow, G.E., 1982. The anorthoclase structures; the effects of temperature and composition. Am. Mineral. 67, 975–996.

Hawthorne, F.C., 1976. The crystal chemistry of the amphiboles; V, the structure and chemistry of arfvedsonite. Canad. Min. 14, 346–456.

Hovis, G.L., Spearing, D.R., Stebbins, J.F., Roux, J., Clare, A., 1992. X-ray powder diffraction and ^{23}Na, ^{27}Al, and ^{29}Si MAS-NMR investigation of nepheline–kalsilite crystalline solutions. Am. Mineral. 177, 19–29.

Kelsey, C.H., McKie, D., 1964. The unit-cell of aenigmatite. Min. Mag. 33, 986–1001.

Kogarko, L.N., 1980. Ore-forming potential of alkaline magmas. Lithos 26, 167–175.

Konnerup-Madsen, J., Rose-Hansen, J., 1984. Composition and significance of fluid inclusions in the Ilímaussaq peralkaline granite, South Greenland. Bull. Mineral. 107, 317–326.

Kunzendorf, H., Nyegaard, P., Nielsen, B.L., 1982. Distribution of characteristic elements in the radioactive rocks of the northern part of the Kvanefjeld, Ilimaussaq intrusion, South Greenland. Rapp.-Grønl. Geol. Unders. 109.

Kunzmann, T., 1999. The aenigmatite–rhoenite mineral group. Eur. J. Mineral. 11, 743–756.

Lange, R.L., Carmichael, I.S.E., 1990. Thermodynamic properties of silicate liquids with emphasis on density, thermal expansion and compressibility. Rev. Miner. 24, 25–64.

Larsen, L.M., 1976. Clinopyroxenes and coexisting mafic minerals from the alkaline Ilímaussaq intrusion, South Greenland. J. Petrol. 17, 258–290.

Larsen, L.M., 1977. Aenigmatites from the Ilímaussaq intrusion, South Greenland: chemistry and petrological implications. Lithos 10, 257–270.

Larsen, L.M., 1981. Chemistry of feldspars in the Ilımuassaq augite syenite with additional data on some other minerals. Rapp.-Grønl. Geol. Unders. 103, 31–37.

Larsen, L.M., Sørensen, H., 1987. The Ilímaussaq intrusion—progressive crystallization and formation of layering in an agpaitic magma. In: Fitton, J.G., Upton, B.G.J. (Eds.), Alkaline Igneous Rocks. Spec. Publ.-Geol. Soc. Lond., vol. 30, pp. 473–488.

Leake, B.E. (Chairman), 1997. Nomenclature of amphiboles. Report of the Subcommittee on Amphiboles of the International Mineralogical Association Commission on New Minerals and Mineral Names. Eur. J. Mineral. 9, 623–651.

Makino, K., Tomita, K., 1989. Cation distribution in the octahedral sites of hornblendes. Am. Mineral. 74, 1097–1105.

Markl, G., Marks, M., Schwinn, G., Sommer, H., 2001. Phase equilibrium constraints on intensive crystallization parameters of the Ilímaussaq complex, South Greenland. J. Petrol. 42, 2231–2258.

Marks, M., 1999. Bestimmung intensiver Parameter während der Kristallisation des Augitsyenites der Ilímaussaq-Intrusion, Südgrönland. Masters thesis, University of Freiburg.

Marks, M., Markl, G., 2001. Fractionation and assimilation processes in the alkaline augite syenite unit of the Ilímaussaq intrusion, South Greenland, as deduced from phase equilibria. J. Petrol. 42, 1947–1969.

Marks, M., Markl, G., 2003. Illimaussaq "en miniature"; closed-system fractionation in an agpaitic dyke rock from the Gardar Province, South Greenland (contribution to the mineralogy of Ilimaussaq no. 117). Min. Mag. 67, 893–919.

Marks, M., Vennemann, T., Siebel, W., Markl, G., 2003. Quantification of magmatic and hydrothermal processes in a peralkaline syenite–alkali granite complex based on textures, phase equilibria, and stable and radiogenic isotopes. J. Petrol. 44, 1247–1280.

Marks, M., Venemann, T., Siebel, W., Markl, G., 2004. Nd-, O-, and H-isotopic evidence for complex, closed-system fluid evolution of the peralkaline Ilímaussaq intrusion, South Greenland. Geochim. Cosmochim. Acta 68, 3379–3395.

Mitchell, R.H., 1990. A review of the compositional variation of amphiboles in alkaline plutonic complexes. Lithos 26, 135–156.

Morogan, V., 1989. Mass transfer and REE mobility during fenitization at Alnö, Sweden. Contrib. Mineral. Petrol. 20, 268–294.

Nicholls, J., Carmichael, J.S.E., 1969. Peralkaline acid liquids: a petrological study. Contrib. Mineral. Petrol. 20, 268–294.

NiWen, Ashworth, J.R., Ixer, R.A., 1991. Evidence for the mechanism of the reaction producing a bournonite–galena symplectite from meneghinite. Min. Mag. 55, 153–158.

Nolan, J., 1969. Physical properties of synthetic and natural pyroxenes in the system diopside–hedenbergite–acmite. Min. Mag. 37, 216–229.

Rock, N.M.S., 1976. Fenitisation around the Monchique alkaline complex, Portugal. Lithos 9, 263–279.

Rubin, J.N., Henry, C.D., Price, J.G., 1993. The mobility of zirconium and other "immobile" elements during hydrothermal alteration. Chem. Geol. 110, 29–47.

Salvi, S., Williams-Jones, A.E., 1990. The role of hydrothermal processes in the granite hosted Zr, Y, REE deposit at Strange Lake, Quebec/Labrador: evidence from fluid inclusions. Geochim. Cosmochim. Acta 54, 2403–2418.

Salvi, S., Fontan, F., Monchoux, P., Williams-Jones, A.E., Moine, B., 2000. Hydrothermal mobilization of high field strength elements in alkaline igneous systems: evidence from the Tamazeght Complex (Morocco). Econ. Geol. 95, 559–576.

Schwinn, G., 1999. Kristallisationsgeschichte und Fluidentwicklung in agpaitischen Gesteinen der Ilímaussaq Intrusion, Südgrönland. Masters thesis, University of Freiburg.

Sood, M.K., Edgar, A.D., 1970. Melting relations of undersaturated alkaline rocks. Medd. Grønl. 12.

Sørensen, H., 1992. Agpaitic nepheline syenites: a potential source of rare elements. Appl. Geochem. 7, 417–427.

Sørensen, H., 1997. The agpaitic rocks — a review. Min. Mag. 61, 485–498.

Sørensen, H., 2001. Brief introduction to the geology of the Ilímaussaq alkaline complex, South Greenland, and its exploration history. Geol. Greenl. Surv. Bull. 190, 7–23.

Thomas, W.M., 1982. Stability relations of the amphibole hastingsite. Am. J. Sci. 282, 136–164.

Upton, B.G.J., Emeleus, C.H., Heaman, L.M., Goodenough, K.M., Finch, A.A., 2003. Magmatism of the mid-Proterozoic Gardar Province, South Greenland: chronology, petrogenesis and geological setting. Lithos 68, 43–65.

Van Baalen, M.R., 1993. Titanium mobility in metamorphic systems: a review. Chem. Geol. 110, 233–249.

Wagner, T., Cook, N.J., 1997. Mineral reactions in sulphide systems as indicators of evolving fluid geochemistry — a case study from the Apollo mine, Siegerland, FRG. Min. Mag. 61, 573–590.